euspen's 19th International Conference & Exhibition, Bilbao, ES, June 2019
www.euspen.eu

Development of an in-situ inspection system for additive manufacturing based on phase measurement profilometry

Yue Liu[1], Zonghua Zhang[3], Liam Blunt[1]*, Grant Saunby[2], Jason Dawes[2], Ben Blackham[2], Hussein Abdul Rahman[4], Chris Smith[5], Feng Gao[1], Xiangqian Jiang[1]

1EPSRC Future Metrology Hub, University of Huddersfield UK. 2. Manufacturing Technology Centre, Coventry, UK. 3. School of Mechanical Engineering, Hebei University of Technology, Tianjin, China. 4. Higher Colleges of Technology, UAE. 5. Reliance Precision, UK.

l.a.blunt@hud.ac.uk

Abstract

Additive manufacturing (AM) of metal powder by electron beam fusion offers significant advantages compared with traditional subtractive manufacturing techniques. AM has developed significantly over recent years and is now widely used in academic and industry, particularly in aerospace and medical device manufacture. AM techniques still have many unsolved challenges, such as the detection of part defects developed during the AM building process. Powder delivery is a process that occurs many thousands of times during the build cycle, consequently the assessment of delivery quality would be important for in-build quality control. This paper describes the development of an inspection system for the powder bed delivery by using phase measurement profilometry. A compensation algorithm for nonlinear effect is investigated in order to improve the accuracy and traceability of the inspection technique. A temporal synchronisation technique is employed to reduce the data capture time down to 2 seconds for each inspection. Additionally a novel calibration method based on a surface fitting algorithm is investigated and employed to reduce the influence of phase error and random noise. The results show the deployed calibration protocol can effectively enhance the inspection accuracy and solve higher harmonic problems. The proposed in-situ inspection technique was deployed on a prototype electron beam melting (EBM) AM machine. An example of excessive powder delivery due to rake damage during a real part build is used to demonstrate the system capability on the actual EBeam machine. Additionally, two examples of excessive powder delivery across areas of the powder bed and the resulting scanning results obtained during the building are shown. Experimental results demonstrate that powder defects can be efficiently inspected with the proposed technique and inspection accuracy is improved significantly by applying the proposed calibration method and compensation algorithm.

Key words: Additive manufacturing, Fringe projection technique, In-situ measurement, surface geometry, Electron beam bed fusion, System calibration.

1.Introduction

Additive manufacturing (AM) techniques for metallic materials has become a practical fabrication technology and has developed in both industrial and academic fields in recent years, AM provides significant advantages for manufacturing complex geometries and internal features by adding powder material one cross-sectional layer at a time[1]. However, there are still many challenges that need to be addressed further such as improving part surface roughness, improving mechanical performance of printed parts, and reducing stress concentrations, defect detection and assessing embedded material discontinuities, as well as reducing inter-build variation[2]. Among these challenges, in-situ defect detection is an important issue. Powder delivery is a significant process which can affect the product quality, because during the melting and resolidification process, cracks and pores can occur within the printed objects due to the low quality or inconsistency of the powder delivery[3]. Hence implementation of an effective monitoring method for assessment of delivery quality during manufacturing is essential to improve manufacturing precision and to enhance product quality[4]. Typical defects include: scores in the powder orthogonal to the blade axis due to powder agglomeration, scores and ridges parallel to the blade direction due to vibrations in the blade, excessive powder delivery due to blade damage or insufficient powder delivery due to too low powder dosage [3,5].

Many researchers and research institutes have investigated a number of in-situ metrology techniques for AM to assess the surface form of the powder bed or printed parts. Berumen *et al.*[6] inspected pores and balling by capturing 2D images with an in-line camera. Hu *et al.*[7] employed a near-infrared (NIR) camera in combination with a powder delivery rate sensor for pool monitoring during powder DED (Directed Energy Deposition) processing. Shrestha *et al.*[8] analysed the surfaces of PB-EBAM-fabricated Ti6Al4V parts by using a white-light interferometer. Li et al.[9] presented a paper to obtain 3D surface topography and 3D contour data of the fusion area using enhanced phase measuring profilometry (EPMP). In summary however, the methods above are either 2D inspection, temperature monitoring, are time consuming, or cover a small field of view. To avoid pores and balling arising from poor powder delivery it is necessary to accurately obtain the geometric information of the whole powder bed or melting surface in order to stop the AM process if necessary. A core requirement for in-situ application of such a metrology technique, is that the system must record information from the powder bed in the period after powder delivery and before powder melting is initiated, where this period is of the order of several seconds. Therefore, it is essential to investigate an inspection method that is i) full field ii) high speed, iii) high

accuracy and iv) has a large field of view (FOV). The fringe projection technique has been widely studied over several years because of its advantages of, full-field, high speed, high accuracy, low cost and large field of view. The accuracy of such systems has been quoted as nanometer to submicrometer for measuring small objects, and some commecial scanners (gom) can achieve less 0.1mm/m accuracy for measuring larger objects circe m^2 [10,11,12,13,14].These advantages would meet the requirements for the in-situ inspection of powder bed and printed parts. Consequently, the application of fringe projection techniques (by convention referred to as phase measurement profilometry) to in process inspection during AM manufacture is reported in this paper.

2.Metrology Technique

A schematic of fringe projection set up is shown in Figure 1. The final implementation was within a new prototype e-beam AM system comprising an e-beam powder melting source, powder delivery system, a powder bed transfer stage and the fringe projection inspection system is shown in Figure 2. The internal environment of the machine is held under a vacuum. Consequently, the inspection system is fixed on top of the machine outside of the vacuum and the powder bed is "viewed" through leaded glass windows, the windows are protected during the powder melting phase by Kapton film. The fringe projection system consists of a CCD (charge-coupled device) camera and a DLP (digital light processing) projector. The position of the projector and the camera were fixed with the angle between the optical axes of circa 30°. The inspected powder surface is at the intersection of the camera/projector axes. The measurement principle of fringe projection is triangulation. During the manufacturing process, a layer of powder is dispensed from a powder hopper. The sinusoidal fringe patterns are generated by a computer and projected onto the surfaces of the powder through the projector. Because of the surface perturbations on the powder surface, the projected fringe patterns are deformed they are then captured by the camera and analysed in order to quantify defects across the full area of the powder bed. The quantified surface geometry information of the detected surface is obtained using the captured data and the system calibration information. The position of projector and camera is fixed and a reference plane M is set. The geometrical relationship between these can be represent by a mathematical relationship between the absolute phase map and depth data[15] as shown in equation 1.

$$Z = \frac{L_0}{\frac{2\pi L_0^2 L\cos\theta}{P_0 \Delta\varphi(x,y)(L_0 + x\cos\theta\sin\theta)^2} - \frac{L\cos\theta\sin\theta}{L_0 + x\cos\theta\sin\theta} + 1} \quad (1)$$

where Z is the height value related to the reference plane M. L is the distance between the CCD camera and the DLP projector. Δϕ is the absolute unwrapped phase difference between the measured surface and the reference surface M. L_0 is the working distance from the camera to the reference surface M. θ is the angle between the optical axes of the projector and the camera and P_0 is the period of the projected fringe pattern on a virtual plane. Therefore, the height values across the surface can be calculated with the phase information and system parameters.

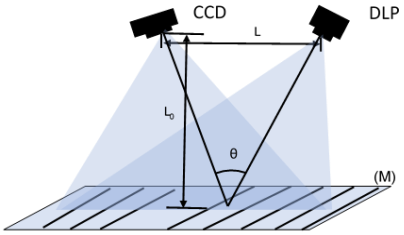

Figure 1. Schematic of fringe projection set up

The of fringe projection system comprises an industrial CCD camera (SVS evo12040MBGEB) with a resolution of 3016x4016 pixels. It supports external and internal trigger. The projector is an industrial digital projector (Light Crafter 4500) with a resolution of 912x1140 micromirror array. Twelve sinusoidal fringe patterns with optimum fringe frenquency of 100, 99 and 90 were generated by software and sequentially projected onto the inspected powder surface. The system parameters can be obtained by system calibration, and the areal shape of the powder surface could be measured by the developed system.

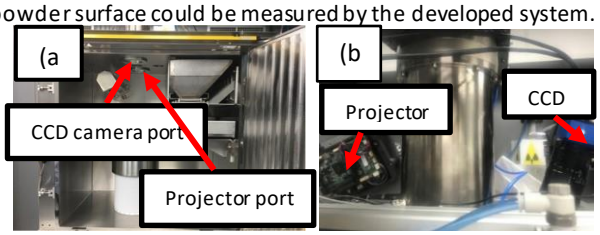

Figure 2. Prototype system with inspection system in a new e-beam system a) internal chamber view, b) external and top of build chamber

2.1. Compensation of nonlinear effect and temporal synchronisation technique

During measurement and system build errors, problems occur that lead to low inspection accuracy. One issue is the nonlinear projection system effect that originates from the projector and the camera, termed the gamma effect. The nonlinear gamma effect will generate system errors, which is manifested as a high harmonic effects in the projection system as shown in Figure 3. A more than five-step phase-shifting algorithm would decrease this nonlinear effect. However, it would decrease measurement speed by using more than five-steps of the phase-shifting algorithm. Therefore, it is important to calibrate out this nonlinear effect.

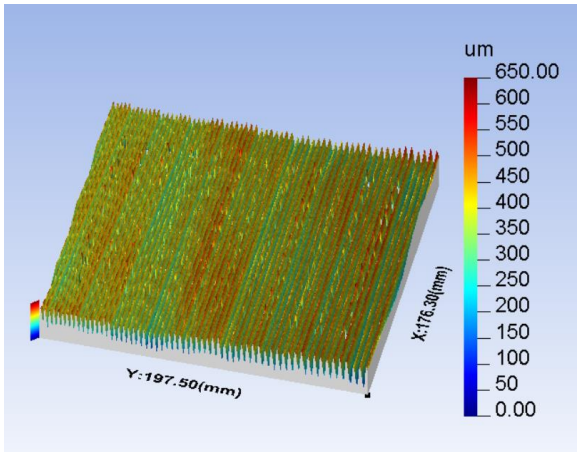

Figure 3. The measurement errors from nonlinear effect and black circle rings

The nonlinear effect is derived from the nonlinear expression of the optical instrument. A projection system uses intensity information to calculate phase information. When the intensity fringe patterns are generated by the software and projected by the projector, the photosensitive components of the projector change the intensity of the projected fringe patterns due to their nonlinear response. This results in a mismatch between the output value and the input value, which results in

measurement error. Similarly, the photosensitive components of the camera also have a nonlinear effect when the camera captures fringe patterns. Because of the nonlinear effect, high-order harmonic effects occur within the collected areal data. A basic gamma translation equation is as follows[16]:

$$Y = x^{\gamma} \quad (1)$$

where x is input intensity and Y is output intensity. γ is the gamma coefficient. γ can change the contrast ratio of different grey value levels. The value of γ determines the mapped relationship between the input intensity and the output intensity of the projection system.

In a sinusoidal projection system, after capturing grey level images, the input intensity can be illustrated with Equation 2. The ideal intensity output is illustrated in Equation 3. However, the relationship between the input intensity and the real output intensity is illustrated in Equation 4.

$$I_{in}(x,y) = I_{DC}(x,y) + I_m(x,y)\cos[\varphi(x,y) + \alpha(x,y)] \quad (2)$$

$$I_{out}(x,y) = I_{DC}(x,y) + I_m(x,y)\cos[\varphi(x,y) + \alpha(x,y)] \quad (3)$$

$$I_{out}(x,y) = I_{DC}(x,y) + I_m(x,y)\cos[\varphi(x,y) + \alpha(x,y)]^{\gamma} \quad (4)$$

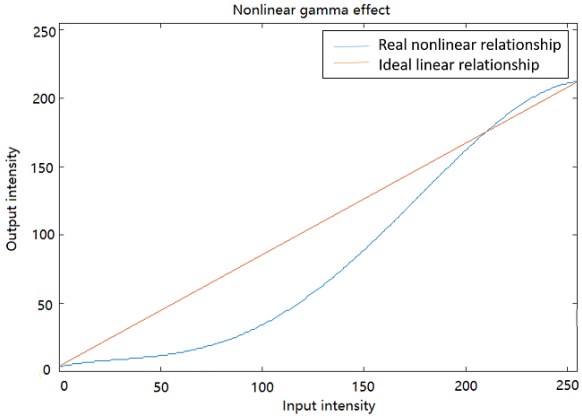

Figure 4. The relationship of input intensity and output intensity

This paper presents a method to compensate the system error by constructing a lookup table (LUT). It is not easy to determine the parameter gamma γ therefore the main method to solve this problem is to find the real relationship between input intensity value and output intensity value. The projector software generates 520 grey level images with an intensity scale from 0 to 255, which are projected and captured by the camera. After calculating the intensity of the captured images, the relationship between the input intensity value and the output intensity value is illustrated as the blue (lower) line as shown in Figure 4. The red line (upper) is the ideal linear relationship and the blue line is the real nonlinear relationship between input intensity and output intensity for this system. Calculating the inverse function of the relationship between input intensity and output intensity generates a LUT to compensate for the nonlinear gamma errors. After building this LUT, the projected intensity images can be cross referenced in the LUT to correct the nonlinear effect.

In order to improve measurement speed and measurement stability, the projector can realize a synchronous function. Two configurable input/output trigger connectors can be connected to realize synchronized image capture. By implementing the synchronous trigger function, the capture speed for the 12 captured images is around 2 seconds. This time is sufficient to capture data between powder delivery and the beginning of the E-beam melting procedure.

2.2. Surface fitting algorithm

During the system calibration (x,y,z axes), a calibration board with certified spacing black circle rings markings is used to obtain absolute phase data at several height positions which are used to calculate system parameters as shown in figure 5 (a). When fringe patterns are projected onto the board, because of the colour of the rings, the captured fringe patterns have low fringe contrast, which results in phase error and measurement error shown as figure 5 (b).

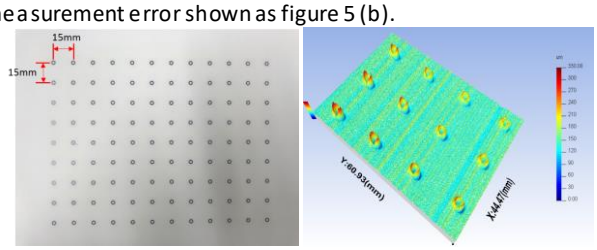

Figure 5. (a) Circle ring calibration board (b) The measurement results of the circle ring calibration board

A calibration approach based on curve fitting is applied to solve this problem. The noisy points are removed by calculating the modulation of the fringe patterns. By setting a threshold value, the outliers and the invalid points having low modulation can be identified. The outliers crossing the circle ring area are then removed. The unwrapped phase map is calculated from the rest of the wrapped phase data by using the optimum 3-frequency selection algorithm[17]. In order to fill in the invalid points, a 5th order polynomial fitting equation is investigated to match the unwrapped phase data as following:

$$\begin{aligned}\text{Phase}(v,u) = {} & P_0(v,u) + P_1(v,u)x + P_2(v,u)y + P_3(v,u)x^2 \\ & + P_4(v,u)xy + P_5(v,u)y^2 + P_6(v,u)x^3 + P_7(v,u)x^2y \\ & + P_8(v,u)xy^2 + P_9(v,u)y^3 + P_{10}(v,u)x^4 + P_{11}(v,u)x^3y \\ & + P_{12}(v,u)x^2x^2 + P_{13}(v,u)xy^3 + P_{14}(v,u)y^4 + P_{15}(v,u)x^5 \\ & + P_{16}(v,u)x^4y + P_{17}(v,u)x^3y^2 + P_{18}(v,u)x^2y^3 + P_{19}(v,u)xy^4 \\ & + P_{20}(v,u)y^5 \end{aligned} \quad (5)$$

where v and u are the pixels positions of the camera coordinate system, x and y are pixels, and P_n is the coefficients of the fitting equation. Because the calibration board is a flat white ceramic plate, the unwrapped phase map of the calibration board is ideally a plane. Theoretically, a linear fitting can determine the plane. Despite the effort of eliminating the distortion of the lens and the non-linearity of the system, uneven fringe projection was still present and this will still distort the unwrapped phase. Therefore, a relatively high order fitting (5th order polynomial) was used. The points with the deviation (noise) between the fitted results and the original data over three times of the standard deviation were removed and discarded. The dataset was then fitted again. This procedure was iterated three times. The experimental results showed that over 98% fitting accuracy was achieved. The new fitted phase maps are used in system calibration calculation. Compared with the unwrapped phase, the fitted data not only suppress the influence of random noise but improves the resolution and accuracy in the vertical direction.

3. Experiments

To evaluate the accuracy of the developed powder surface measurement system, a calibration board was placed at several known positions. At each position, it was measured by an independent interferometer with a resolution of 1 nm and the developed system. The plate was positioned at -2.5 mm and 2.5 mm with respect to the reference plane, an as measured extracted profile is shown in Figure 6. The measured distance obtained by the interferometer was taken as the true value, the measured average distance detected by the inspection system, the absolute error between the measurement results and the true value, the standard deviation across surface, and the repeatability are listed in

Table 1. The maximum absolute error is 6.9 µm. The field of view of this inspection system is 180×180 mm².

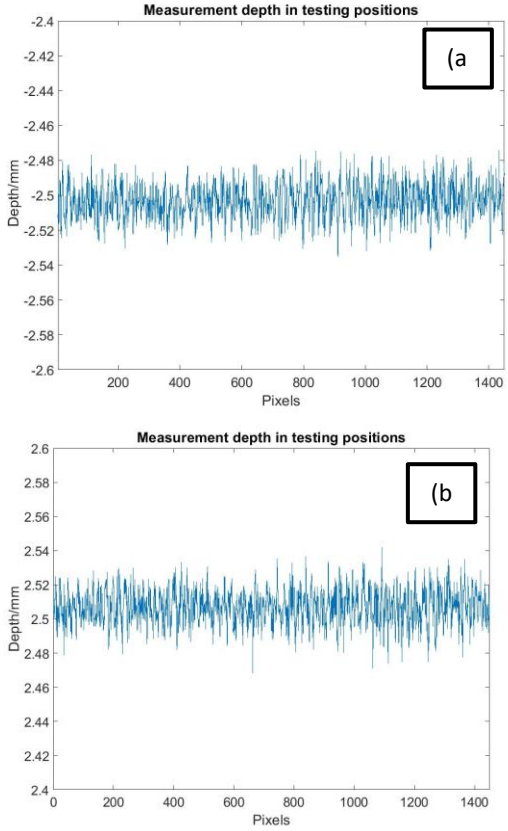

Figure 6. Measured distance along one row near the middle of the white plate, X axis represents the pixel positions, vertical axis is the reconstructed depth of the surface (a) z=-2.5 mm (b) z=2.5mm

Table 1 The experimental results on the measured step Z axis,

Standard positions /mm	Measured average distance /mm	Absolute error /mm	Standard deviation /mm	Repeatability /mm
2.5003	2.5072	0.0069	0.0158	0.0041
-2.5008	-2.5029	0.0021	0.0127	0.0068

To illistrate the system capability an exemplar powder bed (average partide dia of 45 µm) whith is excessive powder delivery across an area of the powder bed and a printed square piece in the powder bed was measured figure 7 . Figure 8 shows an example of excessive powder delivered due to powder rake damage recorded using prototype machine. This image was recorded on the new AM system system during a typical build cycle for 3 rectangular tensile test pieces .

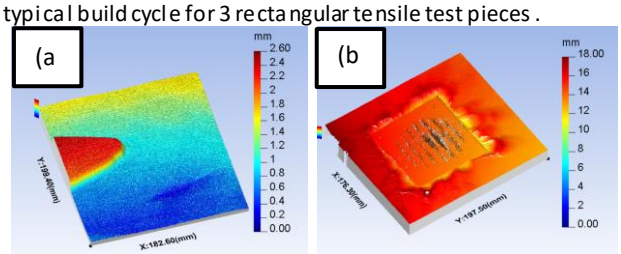

Figure 7. (a) The excessive powder delivery results across area of powder bed (b) scanning results during the building

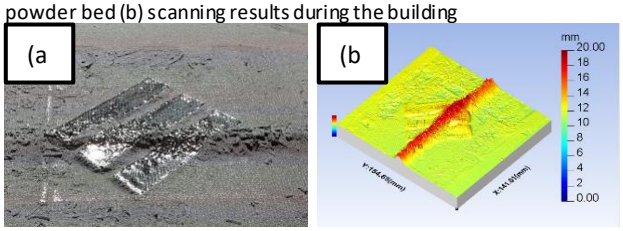

Figure 8. Excessive powder delivery on top of partially build parts (a) Photograph of tested powder (b) 3D results of tested powder

4. Discussion and Conclusion

In summary, this paper investigated and developed an inspection system for the powder bed delivery by using phase measurement profilometry. The system is novel in that it uniquely combines; full field, high speed, high accuracy measurement and combines a novel calibration methodology. A compensation algorithm for nonlinear effects was investigated and implemented in order to improve the accuracy and to solve the high harmonic effects of the inspection system. A temporal synchronisation technique was employed to reduce the dtat capture time to 2 seconds for each inspection. A novel calibration method based on a surface fitting algorithm was investigated and employed to reduce the influence of phase error and random noise. The proposed in-situ inspection technique had been applied to a prototype electron beam melting (EBM) AM machine and exemplar results from the system are given.

References

[1] Townsend A, Senin N, Blunt L, Leach RK and Taylor JS 2016 J. Precision Engineering. 46 34-47

[2] Everton SK, Hirsch M, Stravroulakis P, Leach RK and Clare AT 2016 J. Materials & Design. 95 431-45.

[3] Foster BK, Reutzel EW, Nassar AR, Hall BT, Brown SW and Dickman CJ 2015 C. In Proc. 2015 Solid Freeform Fabrication Symposium. PP 10-12.

[4] Martin KF 1994 J. International Journal of Machine Tools and Manufacture. 34(4) 527-51.

[5] Liu Y, Zhang ZH, Blunt L, Saunby G, Dawes J, Blackham B,et al 2018 C ASPE and euspen Summer Topical Meeting. 69 259-264.

[6] Berumen S, Bechmann F, Lindner S, Kruth JP and Craeghs T 2010 J. Physics procedia. 5 617-22.

[7] Hu D and Kovacevic R 2003 J. International Journal of Machine Tools and Manufacture. 43(1) 51-60.

[8] Shrestha S and Chou K 2017 J. International Journal of Machine Tools and Manufacture. 121 37-49.

[9] Li Z, Liu X, Wen S, He P, Zhong K, Wei Q, Shi Y and Liu S 2018 J. Sensors. 18(4) 1180.

[10] Zhang ZH 2012 J. Optics and Lasers in Engineering. 50(8) 1097-106.

[11] Zhang S, Van Der Weide D and Oliver J 2010 J. Optics express. 18(9) 9684-9.

[12] Zhang S and Yau ST 2006 J. Optics Express.14(7) 2644-9.

[13] Li EB, Peng X, Xi J, Chicharo JF, Yao JQ and Zhang DW 2005 J. Optics express. 13(5) 1561-9.

[14] Chen F, Brown G M and Song M 2000 J. Optical Engineering. 39(1) 10-23.

[15] Zhang Z, Huang S, Meng S, Gao F and Jiang X 2013 J. Optics Express. 21(10) 12218-27.

[16] Guo H, He H and Chen M 2004 J. Applied optics .43(14) 2906-2914.

[17] Zhang Z, Towers CE and Towers DP 2006 J. Optics express. 14(14) 6444-55.